Acta Geochim
https://doi.org/10.1007/s11631-020-00439-x

ORIGINAL ARTICLE

Early Silurian Wuchuan–Sihui–Shaoguan exhalative sedimentary pyrite belt, South China: constraints from zircon dating for K-bentonite of the giant Dajiangping deposit

Yingying Zhang[1,2] · Taiyi Luo[1,3] · Tian Gan[1,2] · Mingzhong Zhou[4] · Xinqiao Han[5]

Received: 27 May 2020 / Revised: 7 September 2020 / Accepted: 30 September 2020

Abstract The Wuchuan–Sihui–Shaoguan (WSS) exhalative sedimentary pyrite belt in the southwestern part of the Qinzhou–Hangzhou (Qin–Hang) belt is the most important sulfur industry base in China. However, a wide range of metallogenetic ages spanning from Ediacaran to Devonian has been reported in the literature. This age range does not support the idea that the typical character of "coeval mineralization" in an exhalative sedimentary mineralization belt in China and worldwide. Therefore, the precise determination of mineralization ages of representative deposits is necessary to provide guides for exploration and metallogenetic models. The Dajiangping pyrite deposit is a typical example of this kind of deposits and is also the largest deposit with a proven reserve of 210 Mt. This deposit was thought to have formed in Ediacaran or Devonian. In this study, 2–3 layers of 10–25 cm thick $2M_1$-type microcrystalline muscovite slate abruptly embedded in the No. IV massive orebody of the deposit has been identified to be low-grade metamorphic K-bentonite. A Concordia zircon LA–ICP–MS U–Pb age of 432.5 ± 1.3 Ma (mean standard weighted deviation of concordance and equivalence = 1.2; N = 11) has been yielded for the low-grade metamorphic K-bentonite. This age is distinctly different from the Rb–Sr isochron age of 630.1 ± 7.3 Ma for siliceous rock at the top of the No. III banded orebody and the Re–Os isochron age of 389 ± 62 Ma for pyrites from a laminated orebody. Instead, it is close to the intercept age (429 Ma) of the youngest detrital zircons from sandstone interlayers of the No. III banded orebody. The Concordia age is also coincident with those of the Late Caledonian (400–460 Ma) magmatism-metamorphism events which are widely distributed in Cathaysia Block. Particularly, it agrees well with that of the Early Silurian extensional volcanism (434–444 Ma) which have been revealed in the Dabaoshan, Siqian–Hekou, and Nanjing volcanic basins in northern Guangdong Province and southern Jiangxi Province. Hence, the dating result in this study confirms that the sedimentary time of the ore-host Daganshan Formation is Early Silurian, and implies that the mineralization age of the Dajiangping pyrite deposit should also be Early Silurian. In combination with the Early Silurian age of Shezui pyrite deposit and the Dabaoshan volcanic basin along the WSS pyrite belt, it could be inferred that the WSS pyrite belt provides a record of the northern expanding of Qinzhou–Fangcheng trough in Early Silurian and that the exhalative pyrite mineralization was triggered by the post-collisional extension of the margin of Cathaysia Block after the intracontinental collision between Cathaysia Block and Yangtze Block during Late Caledonian stage.

Electronic supplementary material The online version of this article (https://doi.org/10.1007/s11631-020-00439-x) contains supplementary material, which is available to authorized users.

✉ Taiyi Luo
luotaiyi@mail.gyig.ac.cn

[1] The State Key Laboratory of Ore Deposit Geochemistry, Institute of Geochemistry, Chinese Academy of Sciences, Guiyang 550081, China

[2] College of Earth and Planetary Sciences, University of Chinese Academy of Sciences, Beijing 101407, China

[3] International Center for Planetary Sciences, College of Geosciences, Chengdu University of Technology, Chengdu 610059, China

[4] School of Geographical and Environmental Sciences, Guizhou Normal University, Guiyang 550001, China

[5] Guangdong Guangye Yunliu Pyrite Mining Co., LTD, Yunfu 527300, China

Published online: 22 October 2020

Keywords Wuchuan–Sihui–Shaoguan exhalative sedimentary pyrite belt · Dajiangping pyrite deposit · Low-grade metamorphic K-bentonite · Zircon U–Pb dating

1 Introduction

Hydrothermal exhalative sedimentary deposits, including sedimentary rock-hosted exhalative deposits (SEDEX) and volcanic rock-hosted massive sulfide (VMS) deposits, are characterized by distinct spatial and temporal distribution (Haitian 1992). As for the mineralization ages and geological settings, they are mostly concentrated in Paleo-Mesoproterozoic (1.9–1.4 Ga) and Early-Middle Palaeozoic (530–300 Ma) eras (Dergachev and Eremin 2008; Zhai et al. 2017) in age, and are known to be accumulated in rift and graben basin settings (Hu et al. 1994; Zaw et al. 2007; Wang et al. 2014; Mortensen et al. 2015). Hydrothermal exhalative sedimentary deposits distribute widely in South China, such as the Middle-Late Proterozoic copper belt (Xiqiu, Luocheng, and Tieshajie), the Late Proterozoic Xinyu-type iron-belt (Yingyangguan, Qidong, and Liangshan), and the Carboniferous pyrite belt (Xinqiao, Shuizhuling, Dongguashan, and Tongguanshan) in the Tongling area of the middle and lower reaches of the Yangtze River, and the Wuchuan–Sihui–Shaoguan (WSS) pyrite belt in Guangdong Province (Hu et al. 1994). The temporal and spatial distribution characteristics of them have been outlined as "coeval mineralization accumulated as a cluster in tectonic junction, deposits clusters grouped as mineralization belt along tectonic boundary" (Hu et al. 1994; Xu et al. 1996). The WSS pyrite belt is situated in the south-western part of the Qinzhou–Hangzhou (Qin–Hang) suture zone. It is one of the most important source bases for the sulphur industry (with a total proven pyrite reserves of ca. 300 Mt) in China (Editorial Board of Discovery History of China Mineral Deposit·Guangdong Volume 1996). A wide metallogenetic age range (Ediacaran–Devonian) for the WSS pyrite belt, including the Dajiangping, Xiniu, and Dabaoshan (only the strati-form pyrite orebody) deposits, has been proposed by previous works, which is inconsistent with the coeval mineralization temporal distribution hypothesis mentioned above. This is an enigma to geologists. Thus, reliable mineralization age for individually representative pyrite deposit from the belt is urgently needed to clarify the temporal issue mentioned above.

The Dajiangping pyrite deposit (with proven reserves of 210 Mt) in Yunfu City in western Guangdong Province, is the largest in the WSS pyrite belt and also in China (Yang et al. 1997). Its mineralization age is still unclear due to a lack of fossils and suitable dating materials in the low-grade metamorphic ore-host strata (the Daganshan Formation). Consequently, various mineralization ages including Early Ediacaran, Middle Devonian, and Lower Devonian have been proposed during exploration in the 1960s (Editorial Board of Discovery History of China Mineral Deposit·Guangdong Volume 1996). Since the 1990s, the Daganshan Formation has been considered to be Ediacaran sequences based on a Rb–Sr isochron age of 630.1 ± 7.3 Ma for the siliceous rocks at the top of the No. III banded orebody (Wang et al. 1996). Recently, some workers considered it to be Middle-Late Devonian in age based on an imprecise pyrite Re–Os isochron age of 389 ± 62 Ma for the laminated ores (Qiu et al. 2018a).

Volcanic zircons preserved in K-bentonites provided most of U–Pb ages in the *International Chronostratigraphic Chart* (Cohen et al. 2013). Given the higher closure temperature (> 900 °C) (Lee et al. 1997) of the zircon U–Pb isotopic system, metamorphic K-bentonites within metamorphic sedimentary strata would be the most valuable candidates for obtaining reliable U–Pb ages for their host sequences. In this study, according to the geological criteria updated by us, we regarded the 10–25 cm thick pyritized silicified slate in the No. IV massive orebody of Dajiangping deposit as a low-grade metamorphic K-bentonite. Moreover, a reasonable zircon U–Pb Concordia age has been yielded to constrain the mineralization age of the Dajiangping deposit and to develop its significances on the related geological events recorded in the WSS pyrite belt.

2 Geological setting

The research area is located in the Yunkai terrane which is controlled by the Wuchuan–Sihui deep fault and the Bobai–Wuzhou fault (the southern prolongation of the Chenzhou–Linwu fault) (Guo et al. 2017; Gan et al. 2018) (Fig. 1a). The basement is composed of widely exposed Precambrian high-grade metamorphic rocks and some Early Palaeozoic low-grade metamorphic rock series (the Yunkai Group), and is unconformably overlain by non-metamorphic Devonian strata (Wang et al. 2013; Zhou et al. 2015). Large-scale Early Palaeozoic igneous rocks are intensively developed in the Cathaysia Block, such as extensive granites in Wuyi, Nanling, and Yunkai areas, and metamorphic intermediate-basic volcanic rocks in Cengxi, Luchuan, and other areas (Wang et al. 2013; Qin et al. 2017).

The Dajiangping pyrite deposit is located 4.5 km northwestern of Yunfu City in Guangdong Province and is close to the eastern margin of the Daganshan dome in the middle-northern part of the Yunkai uplift terrane (Fig. 1b). The mainly ore-controlling structures include the Jianshan inverted anticline, 723 inverted anticline, and the

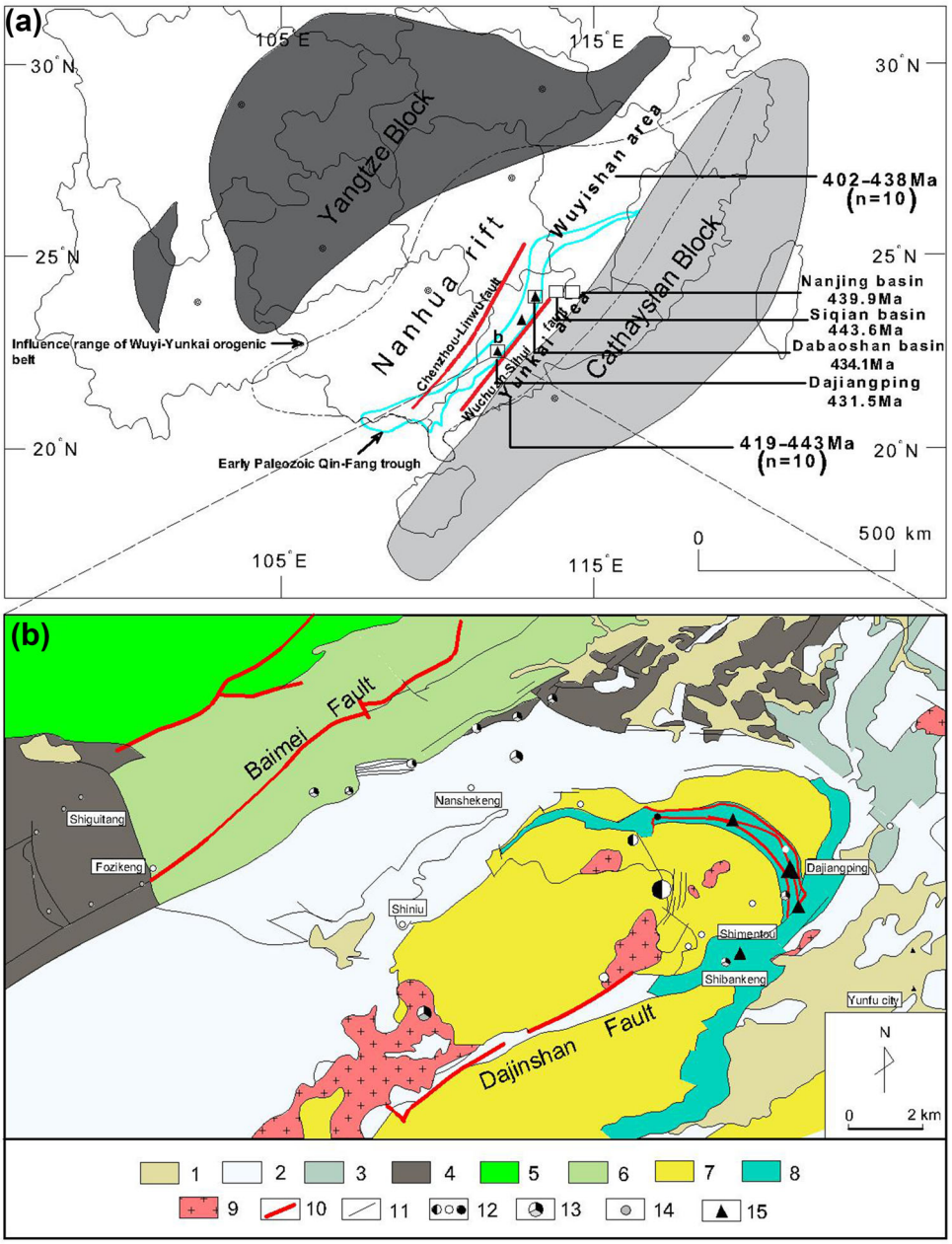

Fig. 1 **a** Sketch-map showing the chronological data of the Wuyi–Yunkai orogenic belt of the Cathaysia Block (modified from Yu et al. 2016; Wang et al. 2018). The Early Paleozoic Qin-Fang trough is blue-green circled from Pan et al. (2016). The data of the Dajiangping pyrite deposit are from this study, whereas the data of the Dabaoshan, Siqian-Hekou, and Nanjing volcanic basins are from Wu et al. (2012), Liu et al. (2018), and Wang et al. (2019). The data for the granite and intermediate-basic volcanic rocks in the Wuyishan area (402–438 Ma; n = 10) and Yunkai area (419–443 Ma; n = 10) are from Wang et al. (2018). **b** Geological and ore resource map of the Daganshan polymetallic ore-field in the west of Guangdong Province (modified from Zhao et al. 2016): (1) Quaternary; (2) Mesozoic Erathem; (3) Carboniferous; (4) Devonian; (5) Silurian; (6) Ordovician; (7) pre-Ediacaran; (8) Ediacaran Daganshan Formation; (9) Yanshanian granite; (10) the main fault; (11) geological boundary; (12) W–Sn, W, and Sn deposits; (13) Ag–Pb–Zn deposits; (14) Cu deposits; (15) pyrite deposits

Dajiangping arcuate fault zone (mainly composed of NE and NNE arcuate faults F_1, F_3, and F_4). The orebodies are held between F_l and F_4 fault and distributed in the core and the western sub-wing of Jianshan inverted anticline (Zeng and Wu 1992). The dominant exposed strata in the open pit are the Daganshan Formation, which is composed of low-grade metamorphic carbonaceous shale, siltstone, tuff, limestone, and pyrite beds (Gan et al. 2018). The massive, lenticular, and banded orebodies are strictly controlled by strata and have been divided into five orebodies (Zeng and Wu 1992), of which the No. IV orebody is the largest and mainly dominated by massive pyrite ores (Editorial Board of Discovery History of China Mineral Deposit·Guangdong Volume 1996). The ore minerals are mostly pyrite with small amounts of pyrrhotite, galena, sphalerite, and chalcopyrite etc. (Xu et al. 1996). The Dajiangping pyrite deposit is a typical SEDEX-type deposit that is faintly superimposed by later magmatic-hydrothermal activity (Song et al. 2011; Qiu et al. 2018b; Gan et al. 2018).

3 Sampling and analytical methods

The No. IV massive orebody of the Dajiangping pyrite deposit is significant for the large dimension (2160 m long; 150 m wide; 70–150 m thick in the middle part and

20–50 m thick in each wing) and high grade of average sulfur content of 37.3 wt% (Editorial Board of Discovery History of China Mineral Deposit·Guangdong Volume 1996). In a residual section of the open pit, the bottom of No. IV orebody is composed of pyritised siltstone and slate, the middle is dominated by massive pyrite (12 m) with some thin layers (10–25 cm) of low-grade metamorphic silicified slate, and the upper part is mainly composed of carbonaceous slate (Fig. 2). Sample 17DJP-20 with weight ca. 25 kg was collected from the middle part of No. IV massive orebody (Fig. 2) (22°58′7″ N, 112°0′48″ E) (Fig. 3a, b). The sample contains quartz (50–60% in volume, the same as below), sericite (30–40%), pyrite (5%), carbonaceous (5%), and occasionally coarse yellow zircons (Fig. 3c).

The separation of zircons, target preparation, and photography of crystal morphology and internal textures (transmittance light, reflected light, and cathodoluminescence) were performed by the Langfang Yuneng Mine and Rock Separation Technical Services Co., Ltd. X-ray diffraction (XRD), bulk rock major and trace element analyses, and laser ablation–inductively coupled plasma mass spectrometry (LA–ICP–MS) U–Pb dating were carried out at the State Key Laboratory of Ore Deposit Geochemistry, Institute of Geochemistry, Chinese Academy of Sciences. The XRD analysis was performed on an Empyrean instrument (PANalytical B.V., Netherlands) and processed with MDI jade 6.0 software. The bulk rock major elements were determined by the melting flaking method on an Axios (PW4400) X-ray fluorescence (XRF) spectrometer (PANalytical B.V., Netherlands) with an accuracy of > 5%. Trace elements were analyzed according to the procedure developed by Qi et al. (2000) on a Plasma Quant-MS Elite (Jena Analytical Instruments Co., Ltd., Germany) with an accuracy of > 10%. The LA–ICP–MS U–Pb analysis was performed using an Agilent 7700x ICP–MS (Agilent Technologies Co., Ltd., USA) with a laser beam spot diameter of 32 μm (Xia et al. 2004). Zircon standard 91500 was used as an external standard for isotope fractionation (Liu et al. 2010), the synthetic silicate glass NIST SRM612 was used as an external standard for elements analyses, and ^{91}Zr was used as the normalization to correct element content (Pearce et al. 1997). The analytical data were processed offline using ICPMS Data Cal (Liu et al. 2008, 2010), and the U–Pb Concordia age and weighted mean ages were calculated by Isoplot 4.15 (Ludwig 2012).

4 Results

Forty zircon grains with clear growth oscillatory zonings in CL images were selected for LA–ICP–MS U–Pb dating (Table 1, Fig. 3e). The selected zircons were subhedral–

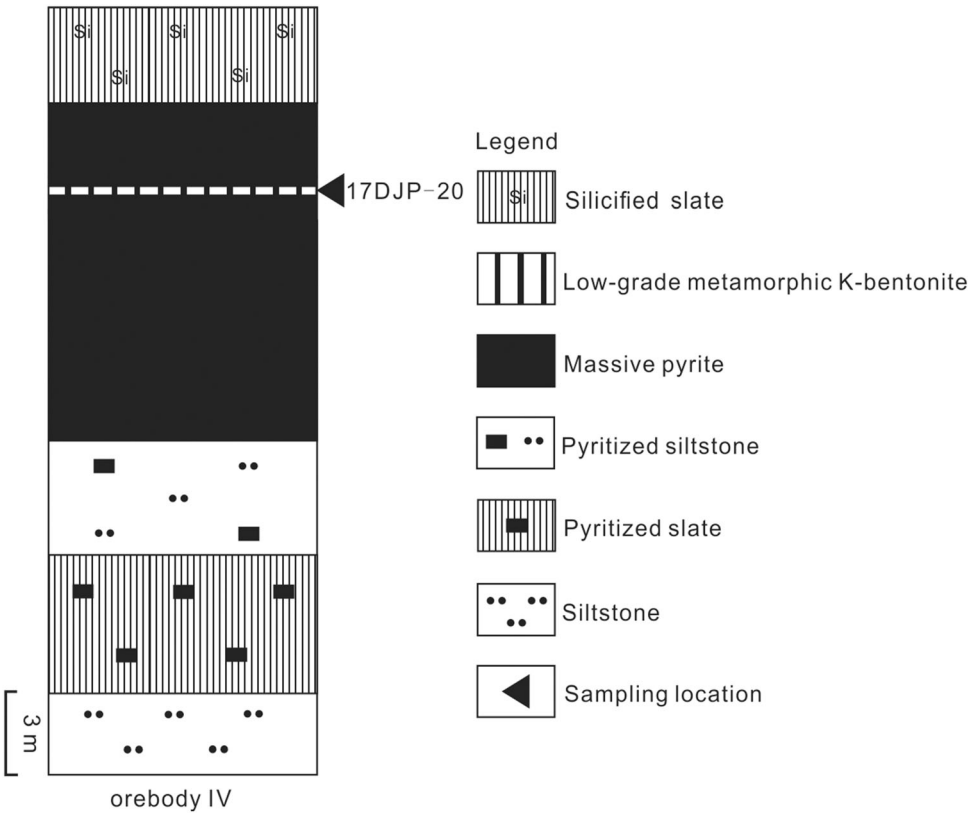

Fig. 2 Schematic stratigraphic column of the Dajiangping pyrite deposit ore-hosting strata (No. IV). The sampling location of for the low-grade metamorphic K-bentonite is also shown (modified from Gan 2017)

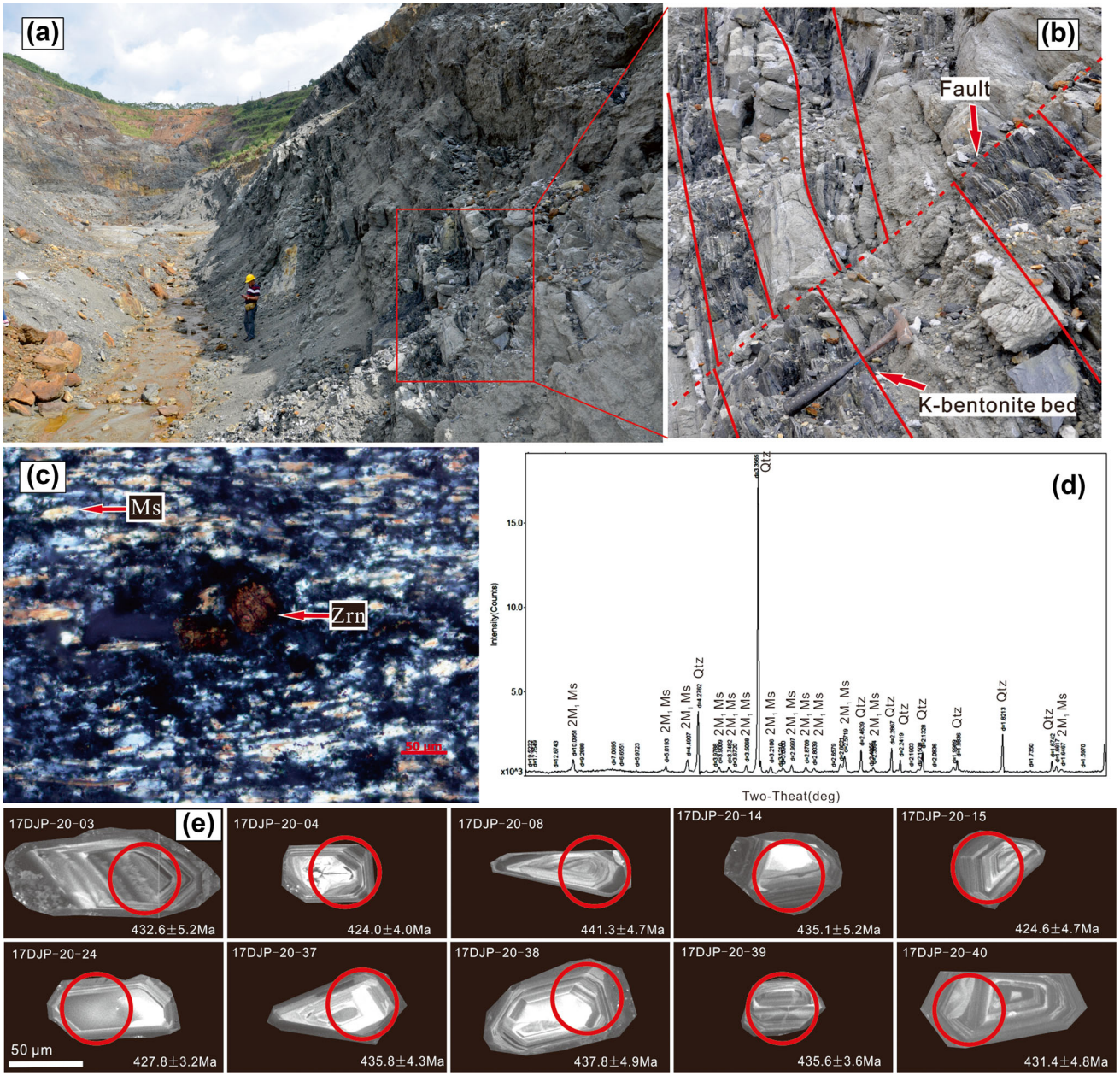

Fig. 3 **a** Field photograph of a distant view of the residual section of the No. IV massive orebody in Dajiangping pyrite deposit. **b** Field photograph of the low-grade metamorphic K-bentonite beds (10–20 cm thick) with late fault. **c** Photomicrographs of the low-grade metamorphic K-bentonite showing parallel foliation of yellow-white microcrystalline muscovite and occasionally coarse yellow zircons. **d** XRD patterns of the low-grade metamorphic K-bentonite (the peaks are the eigenvalues and the corresponding minerals). **e** Cathodoluminescence (CL) images of representative magmatic zircons from the low-grade metamorphic K-bentonite were used for calculating the Concordia age. The circles on the zircons represent the spots for the LA–ICP–MS U–Pb isotope analyses, which are 32 μm in diameter

euhedral, transparent (colorless or yellow), a short prismatic shape, and mostly between 50 and 100 μm in size with an elongation (length-to-width) ratio of between 1 and 3.

For Phanerozoic tuff, zircon ages are often vulnerably disturbed by both positive (from xenocrysts) and negative (from Pb loss) age biases. Ludwig (2012) has suggested a detailed process to deal with such biases. The youngest population of 400–500 Ma of 18 zircons is the main population which is sharp in the plot of the probability density spectrum (Fig. 4b). Getting rid of 5 zircons for heritage or Pb loss biases, a preliminary reliable age of $435.06 + 2.71 - 8.35$ Ma could be extracted from the youngest population (45% of the total zircons) (Fig. 4c). Moreover, after rejecting 2 zircons for a little lower concordance (94%), the remaining 11 zircons yield a

Table 1 LA–ICP–MS zircon U–Pb isotope analyses of the low-grade metamorphic K-bentonite from the Dajiangping pyrite deposit orebody IV

Zircon spot	Th (ppm)	U (ppm)	Th/U	$^{207}Pb^*/^{206}Pb^*$	1σ	$^{207}Pb^*/^{235}U$	1σ	$^{206}Pb^*/^{238}U$	1σ	$^{207}Pb^*/^{206}Pb$ (Ma)	1σ	$^{207}Pb^*/^{235}U$ (Ma)	1σ	$^{206}Pb^*/^{238}U$ (Ma)	1σ	Con%
17DJP-20-01	*299*	*339*	*0.88*	*0.077699*	*0.0014325*	*2.0761*	*0.039810*	*0.19329*	*0.00187*	*1138.9*	*37.0*	*1140.9*	*13.2*	*1139.2*	*10.1*	*99*
17DJP-20-02	*176*	*277*	*0.64*	*0.066712*	*0.0013131*	*1.2537*	*0.026354*	*0.13599*	*0.00155*	*827.8*	*45.4*	*825.1*	*11.9*	*822.0*	*8.8*	*99*
17DJP-20-03	485	919	0.53	0.054035	0.00097014	0.51877	0.010510	0.06941	0.00086	372.3	40.7	424.3	7.0	432.6	5.2	98
17DJP-20-04	163	463	0.35	0.055488	0.0013481	0.52030	0.012307	0.06799	0.00067	431.5	53.7	425.4	8.2	424.0	4.0	99
17DJP-20-05	*457*	*387*	*1.2*	*0.065381*	*0.0011732*	*1.1983*	*0.023080*	*0.13239*	*0.00136*	*787.0*	*41.7*	*799.8*	*10.7*	*801.5*	*7.7*	*99*
17DJP-20-06	*162*	*219*	*0.74*	*0.064750*	*0.0015513*	*1.0958*	*0.027308*	*0.12220*	*0.00119*	*764.8*	*50.0*	*751.3*	*13.2*	*743.2*	*6.9*	*98*
17DJP-20-07	*97.1*	*629*	*0.15*	*0.072750*	*0.0011214*	*1.5914*	*0.024603*	*0.15796*	*0.00128*	*1007.1*	*31.5*	*966.8*	*9.7*	*945.4*	*7.1*	*97*
17DJP-20-08	182	566	0.32	0.056899	0.0012996	0.55586	0.012215	0.07085	0.00077	487.1	51.8	448.8	8.0	441.3	4.7	98
17DJP-20-09	*734*	*787*	*0.93*	*0.068151*	*0.0016119*	*0.62496*	*0.014038*	*0.06634*	*0.00060*	*872.2*	*43.5*	*493.0*	*8.8*	*414.1*	*3.6*	*82*
17DJP-20-10	*443*	*770*	*0.57*	*0.083902*	*0.0013269*	*2.5570*	*0.043853*	*0.21952*	*0.00211*	*1300.0*	*30.7*	*1288.4*	*12.5*	*1279.3*	*11.2*	*99*
17DJP-20-11	*275*	*592*	*0.46*	*0.057520*	*0.0012637*	*0.58574*	*0.013551*	*0.07357*	*0.00091*	*522.3*	*52.8*	*468.1*	*8.7*	*457.6*	*5.5*	*97*
17DJP-20-12	*254*	*332*	*0.76*	*0.064904*	*0.0013711*	*1.2201*	*0.025501*	*0.13585*	*0.00135*	*772.2*	*44.4*	*809.8*	*11.7*	*821.2*	*7.7*	*98*
17DJP-20-13	*711*	*1161*	*0.61*	*0.059273*	*0.0010458*	*0.57756*	*0.0097651*	*0.07038*	*0.00057*	*576.0*	*38.9*	*462.9*	*6.3*	*438.4*	*3.4*	*94*
17DJP-20-14	86.5	661	0.13	0.055664	0.0011427	0.53842	0.012277	0.06982	0.00086	438.9	46.3	437.4	8.1	435.1	5.2	99
17DJP-20-15	356	449	0.79	0.056311	0.0012262	0.53109	0.012089	0.06808	0.00078	464.9	52.8	432.5	8.0	424.6	4.7	98
17DJP-20-16	*416*	*748*	*0.56*	*0.059320*	*0.0012147*	*0.56227*	*0.011306*	*0.06843*	*0.00052*	*588.9*	*16.7*	*453.0*	*7.4*	*426.7*	*3.1*	*94*
17DJP-20-17	*266*	*367*	*0.72*	*0.064956*	*0.0014078*	*1.1141*	*0.023798*	*0.12403*	*0.00115*	*772.2*	*44.4*	*760.2*	*11.4*	*753.7*	*6.6*	*99*
17DJP-20-18	*181*	*616*	*0.29*	*0.16148*	*0.0026847*	*10.321*	*0.18428*	*0.46108*	*0.00473*	*2472.2*	*28.1*	*2464.0*	*16.6*	*2444.3*	*20.9*	*99*
17DJP-20-19	*155*	*530*	*0.29*	*0.075245*	*0.0015045*	*1.8435*	*0.037380*	*0.17722*	*0.00203*	*1075.9*	*39.7*	*1061.1*	*13.4*	*1051.7*	*11.1*	*99*
17DJP-20-21	*191*	*155*	*1.2*	*0.068384*	*0.0019618*	*1.3437*	*0.039580*	*0.14223*	*0.00172*	*879.6*	*59.3*	*864.8*	*17.2*	*857.2*	*9.7*	*99*
17DJP-20-22	*303*	*307*	*0.99*	*0.056867*	*0.0014905*	*0.53065*	*0.014338*	*0.06738*	*0.00070*	*487.1*	*57.4*	*432.2*	*9.5*	*420.3*	*4.2*	*97*
17DJP-20-23	*135*	*218*	*0.62*	*0.11017*	*0.0019320*	*5.1917*	*0.107443*	*0.34035*	*0.00472*	*1802.2*	*32.6*	*1851.3*	*17.7*	*1888.3*	*22.7*	*98*
17DJP-20-24	305	421	0.72	0.054736	0.0013984	0.52066	0.013279	0.06861	0.00053	466.7	57.4	425.6	8.9	427.8	3.2	99
17DJP-20-25	*589*	*434*	*1.4*	*0.059261*	*0.0012600*	*0.74455*	*0.016077*	*0.09079*	*0.00088*	*576.0*	*45.2*	*565.1*	*9.4*	*560.2*	*5.2*	*99*
17DJP-20-26	*265*	*437*	*0.61*	*0.11831*	*0.0017960*	*5.6186*	*0.088888*	*0.34281*	*0.00335*	*1931.5*	*27.2*	*1919.0*	*13.7*	*1900.2*	*16.1*	*99*
17DJP-20-27	*256*	*547*	*0.47*	*0.071856*	*0.0012592*	*1.6038*	*0.029831*	*0.16098*	*0.00164*	*983.3*	*35.2*	*971.7*	*11.7*	*962.2*	*9.1*	*99*
17DJP-20-28	*351*	*483*	*0.73*	*0.093342*	*0.0014926*	*3.1521*	*0.052614*	*0.24329*	*0.00206*	*1494.8*	*30.1*	*1445.5*	*12.9*	*1403.8*	*10.7*	*97*
17DJP-20-29	*120*	*262*	*0.46*	*0.11475*	*0.0020000*	*5.2258*	*0.095586*	*0.32839*	*0.00329*	*1875.6*	*31.5*	*1856.8*	*15.6*	*1830.6*	*16.0*	*98*
17DJP-20-30	*436*	*588*	*0.74*	*0.065314*	*0.0012997*	*1.1292*	*0.024294*	*0.12450*	*0.00135*	*783.3*	*41.5*	*767.4*	*11.6*	*756.4*	*7.7*	*98*
17DJP-20-31	*113*	*377*	*0.30*	*0.068765*	*0.0013791*	*1.4111*	*0.029105*	*0.14805*	*0.00154*	*900.0*	*41.2*	*893.6*	*12.3*	*890.0*	*8.7*	*99*
17DJP-20-32	*91.9*	*135*	*0.68*	*0.061263*	*0.0024603*	*0.61911*	*0.023517*	*0.07353*	*0.00098*	*650.0*	*85.2*	*489.3*	*14.8*	*457.4*	*5.9*	*93*
17DJP-20-33	*121*	*777*	*0.16*	*0.073459*	*0.0011914*	*1.7850*	*0.032294*	*0.17515*	*0.00183*	*1027.8*	*32.3*	*1040.0*	*11.8*	*1040.4*	*10.0*	*99*
17DJP-20-34	*251*	*461*	*0.54*	*0.064496*	*0.0013308*	*1.0938*	*0.021341*	*0.12266*	*0.00099*	*766.7*	*238.9*	*750.4*	*10.4*	*745.8*	*5.7*	*99*
17DJP-20-35	*724*	*812*	*0.89*	*0.059750*	*0.0011539*	*0.59353*	*0.012252*	*0.07157*	*0.00062*	*594.5*	*40.7*	*473.1*	*7.8*	*445.6*	*3.7*	*94*
17DJP-20-36	*696*	*457*	*1.5*	*0.059946*	*0.0013461*	*0.72344*	*0.018003*	*0.08683*	*0.00089*	*611.1*	*48.1*	*552.7*	*10.6*	*536.7*	*5.3*	*97*

Table 1 continued

Zircon spot	Th (ppm)	U (ppm)	Th/U	$^{207}Pb^*/^{206}Pb^*$	1σ	$^{207}Pb^*/^{235}U$	1σ	$^{206}Pb^*/^{238}U$	1σ	$^{207}Pb^*/^{206}Pb$ (Ma)	1σ	$^{207}Pb^*/^{235}U$ (Ma)	1σ	$^{206}Pb^*/^{238}U$ (Ma)	1σ	Con%
17DJP-20-37	146	200	0.73	0.055299	0.0019730	0.53324	0.018659	0.06994	0.00071	433.4	79.6	434.0	12.4	435.8	4.3	99
17DJP-20-38	224	284	0.79	0.055201	0.0016179	0.53660	0.016302	0.07027	0.00082	420.4	64.8	436.2	10.8	437.8	4.9	99
17DJP-20-39	549	694	0.79	0.055440	0.0012536	0.53714	0.012429	0.06991	0.00059	431.5	45.4	436.5	8.2	435.6	3.6	99
17DJP-20-40	427	1011	0.42	0.057467	0.0011538	0.54943	0.011275	0.06921	0.00079	509.3	44.4	444.6	7.4	431.4	4.8	96
17DJP-20-41	364	942	0.39	0.055866	0.0012748	0.54016	0.012305	0.07002	0.00081	455.6	51.8	438.5	8.1	436.3	4.9	99

Pb* indicates the radiogenic portions. Italic shading indicates data rejected from the Concordia age calculations. Spot 17DJP-20-20 spot was not detected due to instrument malfunction

Concordia age of 432.5 ± 1.3 Ma (Mean Standard Weighted Deviation of concordance and equivalence ($MSWD_{CE}$) = 1.2) (Fig. 4d). Weighted mean of $^{206}Pb/^{238}U$ ages (ranging from 424 to 441 Ma) and $^{207}Pb/^{235}U$ ages (ranging from 424 to 448 Ma) of these 11 zircons is 432.4 ± 3.7 Ma (MSWD = 1.6) and 435.0 ± 4.9 Ma (MSWD = 0.99), respectively. These three age groups are highly consistent with certain errors. However, the Concordia age is slightly or significantly more precious than any single U–Pb or Pb–Pb ages and therefore represents the most reliable age for zircon crystallization according to Ludwig (2012).

5 Discussion

5.1 From fallout volcanic ash to K-bentonite

Extensively dispersed fallout volcanic ash, long-distance transported as volcanic ash cloud in the stratosphere, could be a stratigraphic marker in various sedimentary environments (Ninkovich et al. 1978). Take the largest volcanism in Quaternary—the ca. 75 Ka Youngest Toba Tuff (YTT) in Sumatra (Mark et al. 2014) as an example, the relative volcanic ash has been discovered in marine sediments from the Indian Ocean (up to 1.5 m thick) (Pattan et al. 2010), the Arabian Sea (10–38 cm) (Nambiar and Sukumaran 2002) and the South China Sea (2 cm) (Lee et al. 2004), in lacustrine sediments from Malawi Lake in Africa (≤ 1 cm, 7000 km away from Toba caldera) (Lane et al. 2013), in terrestrial deposits from India continental (10 cm) (Blinkhorn et al. 2014) and loess from China (Rao et al. 2007). Based on observations as above, the simulation reveals that ca. 8600 km^3 of magma (ca. 2800 km^3 dense rock equivalents, DRE) had been erupted into the stratosphere within 15 h by a 50–80 km high volcanic ash column, and the volcanic ash clouds gradually deposited in 9–14 days to form a volcanism ash bed with more than 5 mm thick covering ca. 40 million km^2 on the Earth (Lee et al. 2004).

Volcanic ash bed is mainly composed of low-density (1.1 g/cm^3) volcanic glass, which would be easily altered into clay minerals during the hydrolysis and diagenesis process (Christidis and Huff 2009). Altered volcanic ash bed could be further divided into three types: (1) tonstein mainly composed of kaolinite and hosted in coal measures (Dai et al. 2017), (2) bentonite mainly composed of smectite and mostly occurred in the marine strata after the Cretaceous (Christidis and Huff 2009), and (3) K-bentonite mainly composed of illite and illite–smectite (I–S) and mostly occurred in the marine strata before Cretaceous (Huff 2016).

K-bentonite is the most investigated object for stratigraphic chronology. The criteria to distinguish K-bentonite

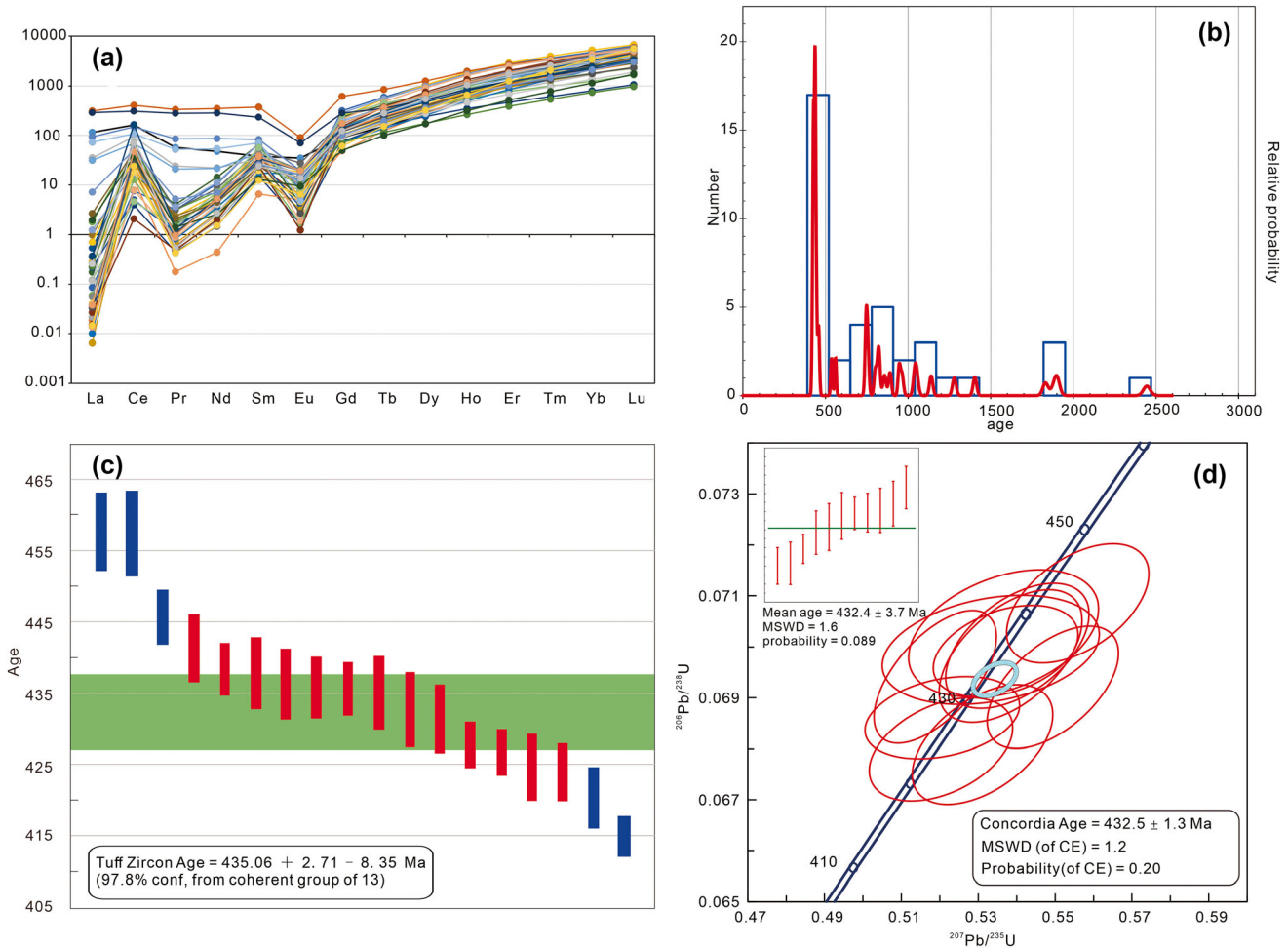

Fig. 4 **a** CI chondrites normalized REE patterns of zircons from the low-grade metamorphic K-bentonite. **b** The age probability density spectrum of the low-grade metamorphic K-bentonite shows that the 400–500 Ma is the main population. **c** Zircon age extractor diagram gives a preliminary reliable age of 435.06 + 2.71 − 8.35 Ma which could be extracted from the youngest population. **d** U–Pb Concordia diagram of magmatic zircons from the low-grade metamorphic K-bentonite

from normal claystone has been summarized by Huff (2008) and emphasized again by Huff (2016). In field investigation, K-bentonite is a fine-grained clay-rich band (1–200 mm) with a slippery and waxy feel when wet. In the laboratory, the main minerals of K-bentonite are smectite and I-S determined by XRD. The heavy minerals separated by wet sieving are typical with volcanogenic minerals (quartz, sanidine, biotite, etc.). However, it should be noted that these heavy minerals may both have volcanic and clastic origin due to the complexity of volcanic magmatic evolution or bioturbation of volcanic ash layers after emplacement.

The criteria established by Huff (2008, 2016) might need to be rectified when K-bentonite had been transformed to silicified claystone, slate or schist caused by later modification (e.g. hydrothermal alteration and regional metamorphism). According to the simulation of the YTT (Lee et al. 2004), the fallout of the volcanic ash cloud formed by giant volcanic eruption may last for several weeks or months. Given the geological time scale, the fallout itself could be depicted as an "instantaneous" deposition of high flux volcanic ash in an extensive area. Therefore, the most essential geological features of a volcanic ash bed (including K-bentonite) should include two aspects. First of all, the volcanic ash bed occurs as a 'sandwich'-like unconformity in a successive sequence, that is, the ash bed is very abruptly embedded into the section, and the lithology and sedimentary facies of the roof and floor rocks are unchanged. The 'sandwich'-like unconformities of K-bentonite have been observed in many Palaeozoic sections, e.g. "white muddy bed" in littoral clastic phosphorite of the Cambrian Meishucun section in China (Zhang et al. 2004); Osmundsberg, Deicke and Millbrig K-bentonites in platform carbonate of Ordovician–Silurian sections in Europe and America (Huff 2016); light-color K-bentonites in deep basin black shale of the Silurian sequence in China (Hu et al. 2009).

Besides, the volcanic ash bed dispersed in a broad area could be a synchronous horizon among different sedimentary environments. For example, the YTT could be a stratigraphic marker in sediments from ocean to continental loess in China and even freshwater lake 7000 km away; and Osmundsberg K-bentonite, one of the most widespread ash beds, could be traced from Sweden across Estonia to the British Isles.

5.2 Discriminating of sample 17DJP-20

The massive pyrite orebody in Dajiangping represents a stable and durative hydrothermal sedimentation environment. However, the abrupt occurrence of the clay beds (low-grade metamorphic slate) exhibits 'sandwich'-like unconformity which seems to be an "instantaneous fallout" of volcanic ash. Laterally, a similar slate with a zircon Concordia age of 433.5 ± 0.64 Ma is also found in the massive pyrite orebody of the Shezui pyrite deposit in Yingde city. Also, a Silurian volcanic ash bed (430.7 ± 4.2 Ma, weighted mean $^{206}Pb/^{238}U$ age, the same below except for the label) has been disclosed in the Lunshan section in Nanjing, Jiangsu Province (Yang et al. 2019). Regionally, large-scale volcanism in Early Silurian has been revealed in the Nanjing (442.1 ± 3.9 and 439.9 ± 3.7 Ma, Liu et al. 2018), Siqian-Hekou (443.6 ± 5.4 Ma, Wu et al. 2012) and Dabaoshan (436.4 ± 4.1, 434.1 ± 4.4 Ma, Wu et al. 2014; 439.1 ± 3.6, 437.1 ± 2.3 and 437.3 ± 2.1 Ma, Wang, et al. 2019) volcanic basins in southern Jiangxi Province and northern Guangdong Province. These evidences clearly show that the intensive Early Silurian volcanism had erupted along the Wuchuan-Sihui deep fault in southwestern periphery of Cathaysia Block. Therefore, it is reasonable that the instantaneous fallout of relative volcanic ash could be recorded in the narrow and long Qin–Fang trough (Pan et al. 2016).

Under microscopic observation (Fig. 3c), the slate 17DJP-20 is mainly composed of microcrystalline quartz (about 50–60% in volume), sericite (about 30–40% in volume) which has been identified to be $2M_1$ type microcrystalline muscovite through XRD analysis (Fig. 3d) and about 10% carbonaceous plus pyrite. Minerals composition of the slate could also be reflected by the major chemical components of SiO_2, Al_2O_3, LOI and K_2O (showing in the appendix table in ESM). Moreover, the molar ratio of Al_2O_3 to K_2O is 2.9, which means that Al_2O_3 and K_2O exist almost in the standard form of muscovite (molar ratio of Al_2O_3 to K_2O is 3). Considering the high SiO_2 content (73.08 wt%) of initial volcanic magma of K-bentonite (Huff et al. 1998) and hydrothermal sedimentation environment, the fallout volcanic ash could be altered to pyritized silicified clay rock in the pyrite mineralization stage. And clay minerals would further transform into $2M_1$ type microcrystalline muscovite to form pyritized silicified slate in later metamorphism.

Zircon is the most stable heavy mineral to resist lower-temperature hydrothermal alteration and shallow metamorphism. Although zircon preserved in ash bed might has complexity sources, the youngest age population of magmatic zircon should represent the relative volcanism (Zhou et al. 2018). 40 sub-euhedral to euhedral zircons with clear growth oscillation zone have been selected as magmatic zircon (Koschek 1993; Corfu et al. 2003), which could be supported by Th/U ratios (Belousova et al. 2002) range from 0.13 to 1.52 and typical left-leaning trend REE patterns (Fig. 4a) with obviously positive Ce anomalies (δCe = 1.1–213) and negative Eu anomalies (δEu = 0.01–0.54) (Hoskin and Ireland 2000). These zircons display a $^{206}Pb/^{238}U$ age spectrum (Fig. 4b) with a high concordance ratio (> 93%, except No. 09 spot of 82%) from 420 to 2444 Ma. The youngest age population (400–500 Ma, n = 18) is very sharp in the age spectrum (Fig. 4b) and a coherent group (n = 11) yields a Concordia age of 432.5 ± 1.3 Ma with suitable $MSWD_{CE}$.

Therefore, based on the criteria suggested by Huff (2008, 2016) and the amendment proposed in this paper, it could be confirmed that the pyritized silicified slate occurred as 'sandwich'-like unconformity in the No. IV massive orebody of the Dajiangping deposit is low-grade metamorphic K-bentonite.

5.3 Caledonian magmatism-thermal event and pyrite mineralization

The siliceous rocks at the top of Dajiangping No. III banded orebody have been dated at 630.1 ± 7.3 Ma using Rb–Sr method (Wang et al. 1996). However, the reliability of such an age cannot be evaluated due to the easy resetting of the low closure temperature of Rb–Sr isotopic system (Nebel 2013). A Re–Os isochron age of 389 ± 62 Ma for the pyrite from the laminated orebodies of the Daijiangping deposit has been determined, and thus the Daganshan Formation is inferred to form during the Middle-Upper Devonian (Qiu et al. 2018a). Nevertheless, higher error makes the Re–Os age a little depreciated.

Both the intercept ages of the youngest detrital zircons from a sandstone interlayer in the laminated orebody (Qiu et al. 2018a) and the Concordia age of magmatic zircons from the modified K-bentonite in the No. IV massive orebody imply that the Caledonian magmatism was recorded in Dajingping pyrite mineralization process. Hence the Daganshan Formation is not an Ediacaran stratum. Expanding with growing abundant zircon chronology data, a huge Caledonian granite belt with ca. 200 granite masses dispersed within a total area ca. 20000 km^2 in South China has been identified (Zhou 2003; Shu and Wang, 2019). Two-

stage granites have been distinguished. The early-stage (460–430 Ma) of I-type granite with foliation texture are typical for small masses and scale, and the main and peak stage (430–400 Ma) of S-type granite are significant for large numbers and broad-scale over 90% area (Shu 2006). Extensive ductile shear deformation and metamorphic zones circled and coupled with the Caledonian granite are the most important constituent of the Caledonian intracontinental orogenic belt (Yu et al. 2007). Combining granite dating with metamorphic minerals dating (e.g. Ar–Ar dating of white mica, biotite, and hornblende, EPMA dating of monazite), Li et al. (2010) suggest that the Wuyi–Yunkai Caledonian orogeny occurred between mid-Ordovician (> 460 Ma) and earliest Devonian (ca. 415 Ma). Therefore, the metamorphic Daganshan Formation should be deposited before 415 Ma.

A curious characteristic of the Caledonian granite in south China, the absence of matching volcanic rocks probably caused by anatexis under compression, has been first summarized by Zhou (2003). Shu (2006) seconded the opinion and emphasized the lack of hydrothermal exhalative sulfide ore deposits in a compression tectonic setting. However, in the last decades, a brief post-collisional extension episode in Early Silurian has been revealed by a series of intermediate-basic volcanic activity in the northern area of Yunkai, including scattered volcanic rocks (420–438 Ma) (e.g. Genzhushan and Chitong) (Xu et al. 2019; Qin et al. 2017; Liu et al. 2018) and a cluster of Caledonian volcanic basins (Nanjing, Siqian-Hekou and Dabaoshan) with zircon U–Pb ages from 434 to 444 Ma occurring along WSS fault at southern Jiangxi Province and Northern Guangdong Province. Based on dating of dacite, the VMS-type pyrite mineralization in the Dabaoshan volcanic basin, which had been determined to Devonian (Ge and Han 1986), has been revised as Early Silurian (Wu et al. 2014).

Due to uplifting of the Cathaysia Block and closing of Nanhua ocean in Caledonian orogeny, there is a broad unconformity between Devonian and Ordovician sequences for the absence of Silurian in many areas of the Cathaysia Block, but only the Qin–Fang trough kept successive sedimentation during Silurian–Devonian (Liu and Xu 1994). During the brief post-collisional extension episode, the north-east Qin–Fang trough further extended toward to the Dabaoshan area and then transformed into west–east volcanic basins in the northern Guangdong and southern Jiangxi regions (Liu and Xu 1994; Hao et al. 2010; Pan et al. 2016). Besides, accompany with activating of the northeast Wuchuan–Sihui deep fault during the extension episode, intensive hydrothermal exhalative sedimentary mineralization occurred (e.g. SEDEX-type Dajiangping and Shezui deposits and VMS-type mineralization in Dabaoshan deposit). Thus, in the Early Silurian of Qin–Fang trough, the low-grade metamorphic K-bentonite in this study represents the matching volcanic event and the giant pyrite mineralization have recorded the brief extension episode of Caledonian orogeny in South China.

6 Conclusions

For modified K-bentonite, the amending geological criteria emphasize the "instantaneous fallout" of ash cloud and the broadly distributing 'sandwich'-like unconformity in strata sequence. Combining mineralogy with geochemistry, some thin silicified slates abruptly embedded in the No. IV massive orebody of the Dajingping pyrite deposit have been identified as low-grade metamorphic K-bentonites. The main and youngest zircon population in one of them yields a Concordia age of 432.5 ± 1.3 Ma ($MSWD_{CE}$ = 1.2, n = 11), which is consistent with the weighted mean $^{206}Pb/^{238}U$ and $^{207}Pb/^{235}U$ ages of 432.4 ± 3.7 Ma (MSWD = 1.6) and 435.0 ± 4.9 Ma (MSWD = 0.99), respectively. Given the Caledonian magmatism-metamorphism event in South China, the mineralization age of the Dajiangping pyrite deposit and the sedimentary time of the Daganshan Formation have been rectified as Early Silurian in this study. In combination with the Early Silurian dating of the Shezui pyrite deposit and the Dabaoshan volcanic basin, the WSS pyrite belt in the south-western part of the Qin–Hang suture zone is inferred to be the Early Silurian exhalative sedimentary mineralization triggered by a transient extensional volcanic episode during the Caledonian orogeny.

Acknowledgements We are indebted to the State Key Laboratory of Ore Deposit Geochemistry at the Institute of Geochemistry, Chinese Academy of Sciences, for their technical support, and to anonymous reviewers for their constructive comments and valuable suggestions, which helped to significantly improve this manuscript. This work was supported by the National Natural Science Foundation of China (Grant Nos. 41873058 and 41462001) and the Natural Science and Technology Foundation of Guizhou Province, China (Grant No. JZ [2015] 2009).

Compliance with ethical standards

Conflict of interest The authors declare that they have no conflict of interest.

References

Belousova EA, Griffin WL, O'Reilly SY, Fisher NI (2002) Igneous zircon: trace element composition as an indicator of source rock type. Contrib Mineral Petrol 143:602–622. https://doi.org/10.1007/s00410-002-0364-7

Blinkhorn J, Smith VC, Achyuthan H, Shipton C, Jones SC, Ditchfield PD, Petraglia MD (2014) Discovery of Youngest Toba Tuff localities in the Sagileru Valley, south India, in

association with Palaeolithic industries. Quat Sci Rev 105:239–243. https://doi.org/10.1016/j.quascirev.2014.09.029
Christidis GE, Huff WD (2009) Geological aspects and genesis of bentonites. Elements 5:93–98. https://doi.org/10.2113/gselements.5.2.93
Cohen KM, Finney SC, Gibbard PL, Fan JX (2013) The ICS international chronostratigraphic chart. Episodes 36:199–204. https://doi.org/10.18814/epiiugs/2013/v36i3/002
Corfu F, Hanchar JM, Hoskin PWO, Kinny P (2003) Atlas of zircon textures. In: Hanchar JM, Hoskin PWO (eds) zircon. Mineralogical Society of America, Washington, DC, pp 469–500. https://doi.org/10.2113/0530469
Dai S, Ward CR, Graham IT, French D, Hower JC, Zhao L, Wang X (2017) Altered volcanic ashes in coal and coal-bearing sequences: a review of their nature and significance. Earth-Sci Rev 175:44–74. https://doi.org/10.1016/j.earscirev.2017.10.005
Dergachev AL, Eremin NI (2008) Volcanogenic massive sulfide and sedimentary-exhalation lead–zinc ore formation during the Earth's history. Dokl Earth Sci 423:1220–1222. https://doi.org/10.1134/s1028334x08080084
Editorial Board of Discovery History of China Mineral Deposit·Guangdong Volume (1996) Discovery history of China Mineral Deposit·Guangdong Volume. Geological Publishing House, Beijing, pp 217–229. **(in Chinese with English abstract)**
Gan T (2017) Study on pyrite mineralization mechanism of Datangpo stage in South China: Dajiangping as an example. Dissertation, Chinese Academy of Sciences. **(in Chinese with English abstract)**
Gan T, Han XQ, Liu PS, Zhang YY, Luo TY (2018) Constraint of extremely heterogeneous sulfur isotopes to the genesis of the Dajiangping pyrite deposit in Guangdong Province, China. Acta Mineral Sin 38:406–419. **(in Chinese with English abstract)**
Ge CH, Han F (1986) Submarine volcanic hydrothermal sedimentary origin of the Dabaoshan iron and polymetallic sulfide deposit. Miner Depos 5:1–12. **(in Chinese with English abstract)**
Guo XY, Zheng Y, Zhou YZ, Niu J, Yu PP (2017) Micro-fabric characteristics of pyrite generations and their implications for genesis of Yunfu pyrite deposit, Qinzhou–Hangzhou metallogenetic belt, South China. Acta Sci Nat U Sunyatseni Nat Sci 56:148–157+164. **(in Chinese with English abstract)**
Haitian S (1992) A general-review of volcanogenic massive sulfide deposits in China. Ore Geol Rev 7:43–71
Hao Y, Li SZ, Jin C, Dai LM, Liu B, Liu LP, Liu X (2010) Caledonian structural characteristics and mechanism in Hunan–Jiangxi–Guangxi Provinces. Geotect Metal 34:166–180. **(in Chinese with English abstract)**
Hoskin PWO, Ireland TR (2000) Rare earth element chemistry of zircon and its use as a provenance indicator. Geology 28:627–630. https://doi.org/10.1130/0091-7613(2000)28%3c627:reecoz%3e2.0.co;2
Hu WX, Gu LX, Xu KQ, Hu SX (1994) Metallogenic regularities and prospecting direction of massive sulphide deposits in South China. Geol Rev 40:513–519. **(in Chinese with English abstract)**
Hu YH, Sun WD, Ding X, Wang FY, Ling MX, Liu J (2009) Volcanic event at the Ordovician–Silurian boundary: the message from K-bentonite of Yangtze Block. Acta Petrol Sin 25:3298–3308. **(in Chinese with English abstract)**
Huff WD (2008) Ordovician K-bentonites: issues in interpreting and correlating ancient tephras. Quat Int 178:276–287. https://doi.org/10.1016/j.quaint.2007.04.007
Huff WD (2016) K-bentonites: a review. Am Mineral 101:43–70. https://doi.org/10.2138/am-2016-5339
Huff WD, Bergstrom SM, Kolata DR, Sun HP (1998) The Lower Silurian Osmundsberg K-bentonite. Part II: mineralogy, geochemistry, chemostratigraphy and tectonomagmatic significance. Geol Mag 135:15–26. https://doi.org/10.1017/S001675689700811X
Koschek G (1993) Origin and significance of the SEM cathodoluminescence from zircon. J Microsc Oxf 171:223–232. https://doi.org/10.1111/j.1365-2818.1993.tb03379.x
Lane CS, Chorn BT, Johnson TC (2013) Ash from the Toba supereruption in Lake Malawi shows no volcanic winter in East Africa at 75 ka. PNAS 110:8025–8029. https://doi.org/10.1073/pnas.1301474110
Lee JK, Williams IS, Ellis DJ (1997) Pb, U and Th in natural zircon. Nature 390:159–162
Lee MY, Chen CH, Wei KY, Iizuka Y, Carey S (2004) First Toba super eruption revival. Geology 32:61–64. https://doi.org/10.1130/G19903.1
Li ZX, Li XH, Wartho JA, Clark C, Bao C (2010) Magmatic and metamorphic events during the early Paleozoic Wuyi–Yunkai orogeny, southeastern South China: new age constraints and pressure-temperature conditions. Geol Soc Am Bull 122:772–793. https://doi.org/10.1130/B30021.1
Liu BJ, Xu XS (1994) Atlas of the lithofacies palaeogeography of southern China (Sinian-Triassic). Science Press, Beijing, pp 10–12. **(in Chinese with English abstract)**
Liu Y, Hu Z, Gao S, Guenther D, Xu J, Gao C, Chen H (2008) In situ analysis of major and trace elements of anhydrous minerals by LA–ICP–MS without applying an internal standard. Chem Geol 257:34–43. https://doi.org/10.1016/j.chemgeo.2008.08.004
Liu Y, Hu Z, Zong K, Gao C, Gao S, Xu J, Chen H (2010) Reappraisement and refinement of zircon U–Pb isotope and trace element analyses by LA–ICP–MS. Chin Sci Bull 55:1535–1546. https://doi.org/10.1007/s11434-010-3052-4
Liu S, Wu JH, Ding H, Huang MH (2018) Zircon U–Pb age of the Caledonian volcanic rocks in Nanjing basin of southern Jiangxi Province and its geological significance. Geol Bull China 37:1905–1919. **(in Chinese with English abstract)**
Ludwig KR (2012) User's manual for Isoplot 3.75: a geochronological toolkit for Microsoft Excel. Berkeley Geochronol Cent Spec Publ 5:1–75
Mark DF, Petraglia M, Smith VC, Morgan LE, Barfod DN, Ellis BS, Pearce NJ, Pal JN, Korisettar R (2014) A high-precision Ar-40/Ar-39 age for the Young Toba Tuff and dating of ultra-distal tephra: forcing of quaternary climate and implications for hominin occupation of India. Quat Geochronol 21:90–103. https://doi.org/10.1016/j.quageo.2012.12.004
Mortensen JK, Gemmell JB, McNeill AW, Friedman RM (2015) High-precision U–Pb zircon chronostratigraphy of the Mount Read Volcanic Belt in Western Tasmania, Australia: implications for VHMS deposit formation. Econ Geol 110:445–468. https://doi.org/10.2113/econgeo.110.2.445
Nambiar AR, Sukumaran PV (2002) Characterisation of Late Pleistocene Tephra in deep sea sediments of Arabian Sea. J Geol Soc India 59:79–88
Nebel O (2013) Rb–Sr dating. In: Rink WJ, Thompson J (Eds.), Encyclopedia of Scientific Dating Methods. Springer, Netherlands, pp. 1–19
Ninkovich D, Shackleton NJ, Abdel-Monem AA, Obradovich JD, Izett G (1978) K–Ar age of the late Pleistocene eruption of Toba, north Sumatra. Nature 276:574–577. https://doi.org/10.1038/276574a0
Pan GT, Lu SN, Xiao QH, Zhang KX, Yin FG, Hao GJ, Luo MS, Ren F, Yuan SH (2016) Division of tectonic stages and tectonic evolution in China. Earth Sci Front 23:9–12. **(in Chinese with English abstract)**
Pattan JN, Prasad MS, Babu EVSSK (2010) Correlation of the oldest Toba Tuff to sediments in the central Indian Ocean Basin.

J Earth Syst Sci 119:531–539. https://doi.org/10.1007/s12040-010-0027-4

Pearce NJG, Perkins WT, Westgate JA, Gorton MP, Jackson SE, Neal CR, Chenery SP (1997) A compilation of new and published major and trace element data for NIST SRM 610 and NIST SRM 612 glass reference materials. Geostand Newslett 21:115–144. https://doi.org/10.1111/j.1751-908X.1997.tb00538.x

Qi L, Hu J, Gregoire DC (2000) Determination of trace elements in granites by inductively coupled plasma mass spectrometry. Talanta 51:507–513. https://doi.org/10.1016/s0039-9140(99)00318-5

Qin XF, Wang ZQ, Gong JH, Zhao GY, Shi H, Zhan JY, Wang Z (2017) The confirmation of Caledonian intermediate-mafic volcanic rocks in northern margin of Yunkai block: evidence for Early Paleozoic paleo-ocean basin in southwestern segment of Qinzhou–Hangzhou joint belt. Acta Petrol Sin 33:791–809. **(in Chinese with English abstract)**

Qiu WJ, Zhou MF, Liu ZR (2018a) Late Paleozoic SEDEX deposits in South China formed in a carbonate platform at the northern margin of Gondwana. J Asian Earth Sci 156:41–58. https://doi.org/10.1016/j.jseaes.2018.01.006

Qiu WJ, Zhou MF, Li X, Williams-Ones AE, Yuan H (2018b) The genesis of the giant Dajiangping SEDEX-type pyrite deposit, South China. Econ Geol 113:1419–1446. https://doi.org/10.5382/econgeo.2018.4597

Rao WB, Luo TY, Li XB, Zhu D, Zhou MZ (2007) Records of the YTT event preserved in the Luochuan loess, north China: evidence from available K and fixed NH4+. Acta Mineral Sin 27:325–329. **(in Chinese with English abstract)**

Shu LS (2006) Predevonian tectonic evolution of South China: from Cathaysian Block to Caledonian period folded orogenic belt. Geol J Chin Univ 12:418–431. **(in Chinese with English abstract)**

Shu LS, Wang B (2019) Research advances on the formation of giant granite zones and the genetic linking with assembly-breakup of continents. Geol J Chin Univ 25:161–181. **(in Chinese with English abstract)**

Song S, Hu K, Wen H, Zhang Y, Li K, Fan H (2011) Molybdenum isotopic composition as a tracer for low-medium temperature hydrothermal ore-forming systems: a case study on the Dajiangping pyrite deposit, western Guangdong Province, China. Chin Sci Bull 56:2221–2228. https://doi.org/10.1007/s11434-011-4536-6

Wang HN, Li HY, Wang YX, Wang HH (1996) Rb–Sr dating of the siliceous rock formation in the Dajiangping massive sulphide deposit, Guangdong Province. Chin Sci Bull 41:1960–1962. **(in Chinese with English abstract)**

Wang L, Long WG, Zhou D (2013) Zircon LA–ICP–MS U–Pb age of Caledonian granites from Precambrian basement in Yunkai area and its geological implications. Geol China 40:1016–1029. **(in Chinese with English abstract)**

Wang CM, Deng J, Carranza EJM, Lai XR (2014) Nature, diversity and temporal-spatial distributions of sediment-hosted Pb–Zn deposits in China. Ore Geol Rev 56:327–351. https://doi.org/10.1016/j.oregeorev.2013.06.004

Wang S, Tao JH, Li WX, Wang AD, Lv PL (2018) Zircon U–Pb geochronology, geochemistry, and Sr–Nd isotopic characteristics of the Maixie biotite-granodiorite pluton in northwestern Jiangxi Province and their implications for petrogenesis. Acta Geol Sin 92:747–768. **(in Chinese with English abstract)**

Wang L, Jin X, Xu D, Cai J, Wang Y (2019) Geochronological, geochemical, and Nd–Hf isotopic constraints on the origin of magmatism in the Dabaoshan ore district of South China. Geol J 54:1518–1534. https://doi.org/10.1002/gj.3248

Wu JH, Xiang YX, Huang GR, Liu XD, Liu S (2012) Caledonian zircon SHRIMP U–Pb age of porphyroclastic lava in northern Guangdong Province and its geological significance. Geol J Chin Univ 18:601–608. **(in Chinese with English abstract)**

Wu J, Wang GQ, Liang HY, Huang WT, Lin SP, Zou YQ, Sun WD, Wang YW (2014) Identification of Caledonian volcanic rock in the Dabaoshan ore-field in northern Guangdong Province and its geological implication. Acta Petrol Sin 30:1145–1154. **(in Chinese with English abstract)**

Xia XP, Sun M, Zhao GC, Li HM, Zhou MF (2004) Spot zircon U-Pb isotope analysis by ICP-MS coupled with a frequency quintupled (213 nm) Nd-YAG laser system. Geochem J 38:191–200. https://doi.org/10.2343/geochemj.38.191

Xu KQ, Wang HN, Zhou JP, Zhu JC (1996) A discussion on the exhalative sedimentary massive sulfide deposits of South China. Geol J Chin Univ 2:2–17. **(in Chinese with English abstract)**

Xu C, Wang YJ, Zhang YZ, Xu WJ, Gan CS (2019) Geochronological and geochemical constrains of Chidong Silurian gabbroic pluton in Yunkai domain and its tectonic implication. Earth Sci 44:1–17. **(in Chinese with English abstract)**

Yang RY, Cao JJ, Kang XG, Kang XG, Yin ZQ (1997) The characteristics and genesis of Yunfu pyrite deposit in Guangdong Province. Acta Sci Nat U Sunyatseni Nat Sci 36:80–84. **(in Chinese with English abstract)**

Yang S, Hu W, Wang X, Jiang B, Yao S, Sun F, Huang Z, Zhu F (2019) Duration, evolution, and implications of volcanic activity across the Ordovician–Silurian transition in the Lower Yangtze region, South China. Earth Planet Sci Lett 518:13–25. https://doi.org/10.1016/j.epsl.2019.04.020

Yu JH, Wang LJ, Wei ZY, Sun T, Shu LS (2007) Phanerozoic metamorphic episodes and characteristics of Cathaysia Block. Geol J China Univ 13:474–483. **(in Chinese with English abstract)**

Yu Y, Huang XL, He PL, Li J (2016) I-type granitoids associated with the early Paleozoic intracontinental orogenic collapse along pre-existing block boundary in South China. Lithos 248:353–365. https://doi.org/10.1016/j.lithos.2016.02.002

Zaw K, Peters SG, Cromie P, Burrett C, Hou ZQ (2007) Nature, diversity of deposit types and metallogenic relations of South China. Ore Geol Rev 31:3–47. https://doi.org/10.1016/j.oregeorev.2005.10.006

Zeng XD, Wu YZ (1992) Deformation of polygenetic compound pyrite deposit of Dajiangping, western Guangdong. Geotect Met 16:163–164. **(in Chinese with English abstract)**

Zhai YL, Wei JH, Li YJ, Li X, Ke KJ (2017) Present situation and research progress of the SEDEX deposit. Geophys Geochem Explor 41:392–401. **(in Chinese with English abstract)**

Zhang JM, Zhu MY, Yang AH, Li GX, Yang JH, Heubeck C (2004) Stratigraphic implications of Sinian-early Cambrian volcanic ash beds on the Yangtze Platform. Prog Nat Sci-Mater 14:71–76. https://doi.org/10.1080/10020070412331343171

Zhao HJ, Yu CF, Han XQ, Zheng W (2016) Magmatic hydrothermal superimposition in Dajiangping S (Pb–Zn) deposit, Guangdong Province: Rb–Sr isochron age and sulfur isotope evidence. Miner Depos 35:795–808. **(in Chinese with English abstract)**

Zhou XM (2003) My thinking about granite of South China. Geol J Chin Univ 9:556–565. **(in Chinese with English abstract)**

Zhou XY, Yu JH, Wang LJ, Shen LW, Zhang CH (2015) Compositions and formation of the basement metamorphic rocks in Yunkai terrane, western Guangdong Province, South China. Acta Petrol Sin 31:855–882. **(in Chinese with English abstract)**

Zhou MZ, Luo TY, Huff WD, Yang ZQ, Zhou GH, Gan T, Yang H, Zhang D (2018) Timing the termination of the Doushantuo negative carbon isotope excursion: evidence from U–Pb ages from the Dengying and Liuchapo formations, South China. Sci Bull 63:1431–1438